Open access • Journal Article • DOI:10.1002/JCP.21719

Adenovirus-mediated hPNPase(old-35) gene transfer as a therapeutic strategy for neuroblastoma. — Source link

Tom Van Maerken, Devanand Sarkar, Franki Speleman, Paul Dent ...+2 more authors

Institutions: Virginia Commonwealth University, Ghent University Hospital, University of California, San Francisco

Published on: 01 Jun 2009 - Journal of Cellular Physiology (NIH Public Access)

Topics: Ribonuclease inhibitor, Cancer cell, Neuroblastoma and Gene expression

Journal of Cellular Physiology

Adenovirus-mediated *hPNPase*$^{old-35}$ gene transfer as a therapeutic strategy for neuroblastoma

Journal:	*Journal of Cellular Physiology*
Manuscript ID:	JCP-08-0476.R1
Wiley - Manuscript type:	Original Research Article
Date Submitted by the Author:	24-Dec-2008
Complete List of Authors:	Van Maerken, Tom; Virginia Commonwealth University, Department of Human and Molecular Genetics; Virginia Commonwealth University, Massey Cancer Center; Ghent University Hospital, Center for Medical Genetics; Ghent University Hospital, Department of Clinical Chemistry, Microbiology and Immunology Sarkar, Devanand; Virginia Commonwealth University, Department of Human and Molecular Genetics; Virginia Commonwealth University, Massey Cancer Center; Virginia Commonwealth University, VCU Institute of Molecular Medicine Speleman, Frank; Ghent University Hospital, Center for Medical Genetics Dent, Paul; Virginia Commonwealth University, Massey Cancer Center; Virginia Commonwealth University, VCU Institute of Molecular Medicine; Virginia Commonwealth University, Department of Biochemistry and Molecular Biology Weiss, William; University of California San Francisco, Department of Neurology Fisher, Paul; Virginia Commonwealth University, Department of Human and Molecular Genetics; Virginia Commonwealth University, Massey Cancer Center; Virginia Commonwealth University, VCU Institute of Molecular Medicine
Key Words:	hPNPaseold-35, gene therapy, neuroblastoma, apoptosis, PEG-3 promoter

Adenovirus-mediated *hPNPase*$^{old-35}$ gene transfer as a therapeutic strategy for neuroblastoma

Tom Van Maerken,[1,2,3,4] Devanand Sarkar,[1,2,5] Frank Speleman,[3] Paul Dent,[2,5,6] William A. Weiss,[7] Paul B. Fisher[1,2,5*]

[1]Department of Human and Molecular Genetics, Virginia Commonwealth University, School of Medicine, Richmond, Virginia

[2]Massey Cancer Center, Virginia Commonwealth University, School of Medicine, Richmond, Virginia

[3]Center for Medical Genetics, Ghent University Hospital, Ghent, Belgium

[4]Department of Clinical Chemistry, Microbiology and Immunology, Ghent University Hospital, Ghent, Belgium

[5]VCU Institute of Molecular Medicine, Virginia Commonwealth University, School of Medicine, Richmond, Virginia

[6]Department of Biochemistry and Molecular Biology, Virginia Commonwealth University, School of Medicine, Richmond, Virginia

[7]Department of Neurology, University of California San Francisco, San Francisco, California

***Correspondence to:** Paul B. Fisher, Department of Human and Molecular Genetics, Massey Cancer Center, VCU Institute of Molecular Medicine, Virginia Commonwealth University, School of Medicine, Sanger Hall Building 11-015, 1101 East Marshall Street,

Richmond, VA 23298. Phone: 804-828-9632; Fax: 804-827-1124; E-mail: pbfisher@vcu.edu.

Running title: *hPNPase*$^{old-35}$-based gene therapy for neuroblastoma

Keywords: *hPNPase*$^{old-35}$, gene therapy, neuroblastoma, apoptosis, *PEG-3* promoter

Number of figures: 6

Number of tables: 1

Abstract

Current treatment options for neuroblastoma fail to eradicate the disease in the majority of high-risk patients, clearly mandating development of innovative therapeutic strategies. Gene therapy represents a promising approach for reversing the neoplastic phenotype or driving tumor cells to self-destruction. We presently studied the effects of adenovirus-mediated gene transfer of human polynucleotide phosphorylase (*hPNPase*$^{old-35}$), a 3′,5′-exoribonuclease with growth-inhibitory properties, in neuroblastoma cells. Transgene expression was driven by either the cytomegalovirus (CMV) promoter or by a tumor-selective promoter derived from Progression Elevated Gene-3 (*PEG-3*). Our data demonstrate that efficient adenoviral transduction of neuroblastoma cells and robust transgene expression are feasible objectives, that the *PEG-3* promoter is capable of selectively targeting gene expression in the majority of neuroblastoma cells, and that *hPNPase*$^{old-35}$ induces profound growth suppression and apoptosis of malignant neuroblastoma cells, while exerting limited effects on normal neural crest-derived melanocytes. These findings support future applications of *hPNPase*$^{old-35}$ for targeted gene-based therapy of neuroblastoma and suggest that combination with the *PEG-3* promoter holds promise for creating a potent and selective neuroblastoma therapeutic.

Introduction

Successful treatment of high-risk neuroblastoma remains a major challenge in pediatric oncology. This neural crest-derived malignancy accounts for approximately 15% of all childhood cancer mortality in the US (Maris et al., 2007). Clinical and biological characteristics, such as age at diagnosis, disease stage, histopathology, tumor cell DNA content (ploidy), and copy number status of the N-*myc* oncogene, allow for stratification of neuroblastoma patients into different risk groups (Brodeur, 2003; Maris et al., 2007). About half of all cases are currently classified as high-risk disease, with a mortality rate exceeding 60%, pointing at a compelling need to develop alternative treatment strategies (Maris et al., 2007).

An intriguing therapeutic opportunity for a number of human diseases may be offered by a group of ribonucleases endowed with cytotoxic, immunosuppressive, antitumor, angiogenic, and aspermatogenic activities. These enzymes are referred to as Ribonucleases with Special Biological Actions or RISBASEs (D'Alessio, 1993), as their functions extend beyond the processing and turnover of cellular RNA and the breakdown of dietary RNA. Such specialized ribonucleases are present from prokaryotes to higher mammals and operate in a variety of biological processes, including interstrain competition in bacteria, prevention of self-pollination in plants, pathogen survival within host tissues, antiparasitic, antifungal and antiviral defense, neovascularization, and antitumor action (D'Alessio, 1993; Youle et al., 1993). Interestingly, two of the best-studied antitumor ribonucleases, onconase and bovine seminal ribonuclease, have shown

profound activity against neuroblastoma both *in vitro* and *in vivo*, even in a context of resistance to conventional chemotherapeutic agents (Cinatl et al., 1999, 2000; Kotchetkov et al., 2000; Michaelis et al., 2007). The molecular basis underlying the cytotoxicity of these ribonucleases is not fully understood, but it is accepted that this activity requires interaction with the cell membrane, internalization by endocytosis, translocation to the cytosol, resistance to the endogenous ribonuclease inhibitor (RI) in the cytosol as well as to extracellular and intracellular proteases, and cleavage of cellular RNA (Benito et al., 2005; Arnold and Ulbrich-Hofmann, 2006). Onconase is the only ribonuclease hitherto evaluated in clinical trials, with promising results (Beck et al., 2008), although some caution is warranted in view of a relatively high renal uptake compared to other ribonucleases (Vasandani et al., 1996) and evidence of acute multifocal proximal renal tubular necrosis in mice treated with onconase (Vasandani et al., 1999).

We previously identified an evolutionary conserved 3′,5′-exoribonuclease, human polynucleotide phosphorylase (*hPNPase*$^{old-35}$), in an overlapping-pathway screen (OPS) aimed at delineation of genes displaying coordinated changes in expression during terminal differentiation of human melanoma cells and cellular senescence of progeroid fibroblasts (Leszczyniecka et al., 2002). Overexpression of *hPNPase*$^{old-35}$ in both processes suggested implication in regulation of cellular growth, and subsequent studies documented a potent and widely applicable growth-inhibitory activity. *hPNPase*$^{old-35}$ is an early IFN-α/β response gene (Leszczyniecka et al., 2002, 2003), and has been shown to play a pivotal role in IFN-β-induced growth inhibition by a remarkable ability to specifically degrade c-*myc* mRNA (Sarkar et al., 2006). Transduction of normal human

melanocytes with an *hPNPase*$^{old-35}$-encoding non-replicating adenovirus induces a growth arrest with distinctive morphological and biochemical characteristics of senescence (Sarkar and Fisher, 2006). In melanoma cells, adenoviral overexpression of *hPNPase*$^{old-35}$ not only provokes a G_1 cell cycle arrest and senescence, but also a pronounced degree of apoptosis (Sarkar et al., 2003). The growth-suppressive effect of *hPNPase*$^{old-35}$ was similarly observed in breast, colon, prostate and pancreatic carcinoma, glioblastoma multiforme, fibrosarcoma, and osteosarcoma (Sarkar et al., 2003; and data not shown). Upregulation of *hPNPase*$^{old-35}$ might also mediate chronic inflammatory pathological processes during aging (Sarkar et al., 2004). The RNase PH (RPH) domains of *hPNPase*$^{old-35}$ are critical in mediating its phenotypic effects (Sarkar et al., 2005). Multiple molecular mechanisms seem to play a role in the growth-inhibitory and proinflammatory activity, including selective degradation of c-*myc* mRNA (Sarkar et al., 2003, 2006), activation of double-stranded RNA-dependent protein kinase (PKR) (Sarkar et al., 2007), and generation of reactive oxygen species with subsequent NF-κB activation (Sarkar et al., 2004).

The present study explores if *hPNPase*$^{old-35}$ could be exploited as a selective and efficacious tool for gene therapy of neuroblastoma. This strategy was pursued using replication-incompetent adenoviruses in which *hPNPase*$^{old-35}$ expression is driven by the CMV minimal promoter (Ad.CMV-*hPNPase*$^{old-35}$) or by the minimal promoter region of Progression Elevated Gene-3, *PEG-3* (Ad.PEG-*hPNPase*$^{old-35}$). The *PEG-3* promoter was found previously to function selectively in diverse cancer cells with limited activity in normal cells, and hence has the potential of cancer-specific targeting of transgene

expression (Su et al., 2005). Our results lend support to the potential use of adenovirus-based *hPNPase*$^{old-35}$ delivery in the treatment of neuroblastoma.

Materials and Methods

Cell lines and culture conditions

Human neuroblastoma cell lines IMR-32, NGP, SHEP and SK-N-SH were kindly provided by Dr. R. Versteeg (University of Amsterdam, The Netherlands), and SK-N-BE(2c) human neuroblastoma cells by Dr. J. Lunec (University of Newcastle, UK). Human DU-145 prostate carcinoma cells were purchased from the American Type Culture Collection (Manassas, VA). An SV40 T-antigen immortalized human foreskin melanocyte cell line, FM-516-SV, was initially provided by Dr. L. Diamond (Wistar Institute, PA). The present studies used a subclone of FM-516-SV cells (Sarkar et al., 2006). All cells were cultured as described (Van Maerken et al., 2006).

Adenoviral vector construction, virus production and infection protocol

The recombinant replication-defective adenoviruses, Ad.CMV-*GFP* (green fluorescence protein [GFP] expression driven by CMV promoter), Ad.CMV-*hPNPase*$^{old-35}$ (hemagglutinin [HA]-tagged *hPNPase*$^{old-35}$ expression driven by CMV promoter), and Ad.PEG-*hPNPase*$^{old-35}$ (HA-tagged *hPNPase*$^{old-35}$ expression driven by *PEG-3* promoter), were created by cloning the transgene into a shuttle vector followed by homologous recombination in *E. coli* of the shuttle vector with an adenoviral vector in which the E1 and E3 regions have been deleted, as described previously (Leszczyniecka et al., 2002; Holmes et al., 2003). Production of viral particles in HEK293 cells, virus purification, and titration were performed as described (Holmes et al., 2003). Adenoviral infection of cells, 24 h after plating, was performed at the indicated multiplicity of infection (MOI) in

a minimal volume of serum-free RPMI 1640 medium for 3 h at 37 °C, with rocking of the plates every 15 min, followed by replenishment of complete medium and incubation at 37 °C for the indicated times. The empty adenoviral vector, Ad.*vec*, was used as a control.

Flow cytometric analysis of GFP expression

Cells were seeded in 6-well plates (2.5×10^5 cells per well), incubated for 24 h, and infected with Ad.CMV-*GFP* at an MOI of 0, 12.5, 25, 50, 100 or 200 plaque-forming units (pfu) per cell. After 24 h, cells were harvested by trypsinization, washed with phosphate-buffered saline (PBS), and analyzed for the expression of GFP on a FACSCalibur flow cytometer (BD Biosciences, San Jose, CA) equipped with CellQuest Pro acquisition and analysis software version 5.2 (BD Biosciences). The percentage of GFP-positive cells was quantified using FlowJo version 8.5.3 for Macintosh (Tree Star, Ashland, OR).

Detection of coxsackie-adenovirus receptors (CAR) on the cell surface

Quantification of surface expression of CAR was performed as described previously (Lebedeva et al., 2002). Briefly, cells were incubated with mouse monoclonal anti-CAR antibody for 1 h at 37 °C (1:1000 dilution; Millipore, Billerica, MA), washed, exposed to fluorescein isothiocyanate (FITC)-conjugated anti-mouse immunoglobulins (1:1000 dilution; Sigma, St. Louis, MO) for 1 h at 37 °C in the dark, washed again, and analyzed on a FACSCalibur using CellQuest Pro version 5.2 (BD Biosciences). Unstained cells, cells stained with secondary antibody only, and cells incubated with isotype control

primary antibody followed by secondary antibody were used as controls. Acquired data were analyzed in FlowJo version 8.5.3 for Macintosh (Tree Star) using two evaluation methods. The peak shift was calculated as the difference in peak channels between the cells stained with anti-CAR antibody and the control cells with the highest FITC signal intensity, relative to the position of the peak channel of these control cells. The second method used the Kolmogorov-Smirnov two-sample test for analysis of the flow cytometric histograms (Young, 1977). This test computes, starting from the histograms, the cumulative distribution function of fluorescence intensity for each sample and determines the difference between the cumulative distribution functions, with the *D* value indicating the greatest difference between the two curves.

Analysis of the number of viable cells

Cells were seeded in 96-well tissue culture plates (5×10^3 cells per well), incubated for 24 h, and infected in quadruplicate wells with different adenoviruses at 100 pfu/cell. At 1, 3 and 5 days postinfection, the medium was carefully replaced by fresh medium containing 0.5 mg/mL MTT (Calbiochem, San Diego, CA), followed by incubation of the cells at 37 °C for 4 h and then addition of an equal volume of solubilization solution (0.01 HCl in 10% sodium dodecyl sulfate [SDS]) to each well. The absorbance of the wells was read at 595 nm with a Bio-Rad Model 550 microplate reader (Bio-Rad, Hercules, CA). Each condition was tested in three independent experiments.

Cell cycle and hypodiploidy analysis

Cells were plated in 10-cm dishes (1×10^6 cells per dish) and infected the next day with different adenoviruses at 100 pfu/cell. Measurement of cell cycle phase distribution and hypodiploid DNA content was performed at 2, 3, 4 and 5 days postinfection. Cells were trypsinized, washed 2 × with PBS, and fixed in 70% ethanol overnight at –20 °C. The cells were subsequently washed 2 × with PBS, treated with 0.5 mg/mL RNase A at 37 °C for 30 min, and incubated with 0.1 mg/mL propidium iodide at room temperature for 30 min. Cellular DNA content was measured with a FACSCalibur using CellQuest Pro version 5.2 (BD Biosciences). Cell cycle fractions and the apoptotic A_0 population were quantified using FlowJo version 8.5.3 for Macintosh (Tree Star).

Analysis of caspase-3 and caspase-7 activity

Cells were seeded in 96-well tissue culture plates (5×10^3 cells per well), incubated for 24 h, and infected in triplicate wells with different adenoviruses at 100 pfu/cell. The combined activity of caspase-3 and caspase-7 was measured at 2 and 3 days postinfection using the Caspase-Glo 3/7 assay (Promega, Madison, WI) and a Modulus microplate luminometer (Turner BioSystems, Sunnyvale, CA).

Western blot analysis

Protein lysates were prepared on ice in RIPA buffer (Sigma) containing protease and phosphatase inhibitor cocktails (Roche, Mannheim, Germany), and clarified by centrifugation at 16,000 × g for 15 min at 4 °C. Protein concentrations were determined using the Bradford assay (Bio-Rad). Aliquots containing 25 µg of total protein were resolved by electrophoresis on 8% SDS-polyacrylamide gels, transferred to 0.2 µm

nitrocellulose membranes (Pall Corporation, East Hills, NY), and probed with mouse monoclonal antibodies against HA (1:2000 dilution; Covance, Berkeley, CA) and EF1α (1:1000 dilution; Millipore). Horseradish peroxidase (HRP)-conjugated goat anti-mouse immunoglobulins (1:5000 dilution; Sigma) were used as secondary antibodies. Bands were visualized using ECL Plus detection reagents (Amersham Biosciences, Piscataway, NJ) according to the manufacturer's instructions.

Real-time quantitative reverse transcription-polymerase chain reaction (RT-PCR)

Total RNA was extracted from cells using the RNeasy Mini Kit (Qiagen, Valencia, CA), with RNase-free DNase I treatment on column. After an additional RQ1 DNase treatment in solution (Promega), first-strand cDNA was synthesized from 2 µg total RNA using the iScript cDNA synthesis kit (Bio-Rad). Relative mRNA expression levels were determined using an optimized two-step SYBR Green I real-time quantitative RT-PCR assay with minor modifications (Vandesompele et al., 2002a). Primer sequences are available in the public RTPrimerDB database (http://medgen.ugent.be/rtprimerdb/) (Pattyn et al., 2003, 2006): *GAPDH* [RTPrimerDB ID 3], *SDHA* [7], *UBC* [8], *NEFH* [3504], *NEFL* [3505], *NEFM* [3507], and *CHAT* [3502]. The PCR was run on a LightCycler 480 instrument (Roche) in duplicate reactions of 7.5 µL, containing 250 nM of each primer and cDNA equivalent to 20 ng of total RNA. Gene expression levels and PCR efficiency, along with its standard error, were calculated using qBase*Plus* 1.0 analysis software (http://www.biogazelle.com) (Hellemans et al., 2007), which employs a delta-Ct relative quantification model with PCR efficiency correction and multiple

reference gene normalization (Vandesompele et al., 2002b). Expression levels of *GAPDH*, *SDHA* and *UBC* were used for normalization.

Results

Adenoviral transduction efficiency of neuroblastoma cells and expression of coxsackie-adenovirus receptors (CAR) on the cell surface

To determine the infectivity of neuroblastoma cells by adenoviral vectors and the efficiency of transgene expression, cells were infected with a recombinant replication-defective adenovirus expressing GFP under control of the CMV promoter (Ad.CMV-*GFP*) at various MOIs (ranging from 12.5 to 200 pfu/cell) and monitored for the expression of GFP 24 h postinfection using flow cytometry. Transduction efficiency was assessed by calculating the percentage of cells expressing GFP. This analysis was performed on five human neuroblastoma cell lines [IMR-32, NGP, SHEP, SK-N-BE(2c), and SK-N-SH], on normal human melanocytes immortalized by SV40 T-antigen (FM-516-SV), and on human DU-145 prostate carcinoma cells. The immortalized melanocytes were chosen as a reference point in this study, as they share a common embryonic origin with neuroblastoma cells and as the exact normal counterparts for this malignancy, human fetal neuroblasts, are not available due to ethical and technical considerations. The DU-145 cells were included as a positive control, since these cells are characterized by a high level of surface expression of CAR proteins, which mediate adenovirus attachment and uptake in cells, and accordingly by an excellent adenoviral infectivity (Lebedeva et al., 2003). As shown in Figure 1, the adenoviral transduction efficiency of neuroblastoma cells was MOI-dependent and comparable to that obtained with the DU-145 prostate carcinoma cells. At an MOI of 200 pfu/cell, transduction efficiency ranged from 62% to 88% for neuroblastoma cells [percentage of cells positive for GFP expression: SK-N-

BE(2c), 62%; NGP, 63%; IMR-32, 66%; SK-N-SH, 86%; SHEP, 88%] and was 83% for DU-145 cells. A slightly lower transduction efficiency was recorded for FM-516-SV immortalized melanocytes (55% of cells positive for GFP expression at 200 pfu/cell).

We next investigated the expression of CAR on the cell surface by flow cytometry using monoclonal antibodies against CAR (Table 1). Surface expression of this receptor was detectable for all seven cell lines in this study, as evidenced by the Kolmogorov-Smirnov two-sample test for analysis of flow cytometric histograms ($P<.001$ for each cell line). Analysis of the peak shift in fluorescence signal after staining with anti-CAR antibody and FITC-conjugated secondary antibody indicated the following order of surface CAR number and availability: DU-145 > IMR-32 > NGP > SHEP > SK-N-SH > SK-N-BE(2c) > FM-516-SV. Based on these results, it is obvious that a simple correlative relationship does not exist between surface CAR levels and GFP expression after exposure of cells to Ad.CMV-*GFP*, suggesting a differential regulation of transgene expression after virus entry.

Taken together, these data indicate that efficient adenoviral infection and transgene expression is achievable in neuroblastoma cells, and support the development of adenovirus-mediated gene therapy approaches for neuroblastoma.

Expression of *hPNPase*$^{old-35}$ in FM-516-SV and neuroblastoma cells following adenoviral gene transfer

For assessment of the therapeutic potential of adenovirus-based *hPNPase*$^{old-35}$ delivery for the treatment of neuroblastoma, we decided to explore both the effects of a classical gene expression vector as well as of gene transfer under control of a promoter with cancer-specific properties. Previous studies in multiple tumor models, including human breast carcinoma, glioblastoma multiforme, pancreatic carcinoma and prostate cancer, demonstrated a significantly higher activity of the *PEG-3* promoter in tumor cells compared to their normal counterparts (Su et al., 2005; Chan et al., 2008). We constructed two replication-incompetent adenoviruses, Ad.CMV-*hPNPase*$^{old-35}$ and Ad.PEG-*hPNPase*$^{old-35}$, in which *hPNPase*$^{old-35}$ expression is driven by the CMV minimal promoter and by the minimal promoter region of *PEG-3*, respectively. The *hPNPase*$^{old-35}$ transgene was engineered to encode a hemagglutinin (HA)-tag at the COOH-terminus for monitoring expression. To determine the optimum MOI of Ad.CMV-*hPNPase*$^{old-35}$ and Ad.PEG-*hPNPase*$^{old-35}$ infection, neuroblastoma and FM-516-SV cells were infected at 25, 50, 100 and 200 pfu/cell, and transgene expression was measured by Western blot analysis using an anti-HA antibody. The empty adenoviral vector, Ad.*vec*, was used as a control.

As illustrated in Figure 2, infection with Ad.CMV-*hPNPase*$^{old-35}$ induced an MOI-dependent expression of *hPNPase*$^{old-35}$ in both FM-516-SV immortalized melanocytes and neuroblastoma cells. In contrast, infection with Ad.PEG-*hPNPase*$^{old-35}$ did not result in *hPNPase*$^{old-35}$ expression in FM-516-SV cells, while the degree of transgene expression in neuroblastoma cells after incubation with this adenovirus was variable, ranging from weak HA bands in SHEP and SK-N-BE(2c) cells to a pronounced dose-

dependent expression in IMR-32, NGP and SK-N-SH cells. These results validate the functionality of both constructed *hPNPase*$^{old-35}$-encoding adenoviral vectors and demonstrate that the *PEG-3* promoter is capable of selectively targeting gene expression in the majority of human neuroblastoma cells. We selected 100 pfu/cell as the optimal working concentration for further experiments, as infection with Ad.CMV-*hPNPase*$^{old-35}$ and Ad.PEG-*hPNPase*$^{old-35}$ at 200 pfu/cell resulted in markedly rapid cell death.

Selective growth suppression by Ad.CMV-*hPNPase*$^{old-35}$ and Ad.PEG-*hPNPase*$^{old-35}$ in neuroblastoma cells

We next addressed whether adenovirus-mediated *hPNPase*$^{old-35}$ gene transfer could selectively inhibit the growth of neuroblastoma cells. We therefore infected FM-516-SV melanocytes and neuroblastoma cells with Ad.*vec*, Ad.CMV-*hPNPase*$^{old-35}$ and Ad.PEG-*hPNPase*$^{old-35}$ at 100 pfu/cell, and monitored the number of viable cells by MTT assay at 1, 3 and 5 days postinfection. As depicted in Figure 3, infection with Ad.CMV-*hPNPase*$^{old-35}$ and Ad.PEG-*hPNPase*$^{old-35}$ resulted in a pronounced suppression of growth of IMR-32, NGP, SK-N-BE(2c) and SK-N-SH cells. These growth-inhibitory effects became apparent from 3 days after infection, and were most prominent at day 5. It should be noted that exposure to the empty adenoviral vector, Ad.*vec*, also resulted in some growth inhibition of these cells, but this effect was considerably smaller than the decrease in cell number induced by the *hPNPase*$^{old-35}$-encoding adenoviruses [additional degree of growth suppression due to the transgene component, relative to the number of Ad.*vec*-infected cells, at day 5 postinfection: 50-60% for IMR-32, NGP and SK-N-SH cells, and 20-30% for SK-N-BE(2c) cells]. On the contrary, transduction of SHEP neuroblastoma

cells and FM-516-SV melanocytes with Ad.CMV-*hPNPase*$^{old-35}$ and Ad.PEG-*hPNPase*$^{old-35}$ resulted in only a slight decrease in the number of viable cells at day 5 postinfection.

Taken together, these findings suggest that both Ad.CMV-*hPNPase*$^{old-35}$ and Ad.PEG-*hPNPase*$^{old-35}$ have the ability to suppress the growth of most human neuroblastoma cells. The observation that infection with Ad.CMV-*hPNPase*$^{old-35}$ exerted only a limited growth-inhibitory effect on FM-516-SV immortalized normal melanocytes, despite a distinct induction of *hPNPase*$^{old-35}$ expression, supports the notion of *hPNPase*$^{old-35}$ as a tumor-selective growth-suppressive gene and hence as a valuable gene therapy tool for the treatment of cancer.

Effects of adenoviral infection and *hPNPase*$^{old-35}$ expression on cell cycle progression, apoptosis, and neuronal differentiation of neuroblastoma cells

To investigate the mechanism of growth inhibition, cellular effects of adenovirus-mediated *hPNPase*$^{old-35}$ expression were studied in detail in two well-responsive neuroblastoma cell types, NGP and SK-N-SH, and in the poorly responsive SHEP cells. Flow cytometric cell cycle profiling of NGP cells indicated that infection with Ad.CMV-*hPNPase*$^{old-35}$ and Ad.PEG-*hPNPase*$^{old-35}$ at 100 pfu/cell resulted in a decrease of cells in the S phase, reflective of inhibition of DNA synthesis (Fig. 4A). At early timepoints after infection, this change was mainly accompanied by accumulation of NGP cells in the G_1 phase, while a gradual increase in the sub-G_1 (A_0) population of cells at day 4 and 5 postinfection indicated the occurrence of apoptotic cell death. Infection of NGP cells with

Ad.*vec* at 100 pfu/cell induced a comparable G_1 cell cycle arrest, but only a mild degree of apoptosis. The response of SK-N-SH cells to adenovirus-mediated *hPNPase*$^{old-35}$ gene transfer was characterized by a more extensive and more rapid induction of apoptosis, as evidenced by the A_0 fraction, with an initial arrest at the G_1/S boundary still observable after Ad.PEG-*hPNPase*$^{old-35}$ infection (Fig. 4B). The empty adenoviral vector, Ad.*vec*, also elicited an inhibition of the G_1/S transition in SK-N-SH cells, but only a modest increase in hypodiploid DNA content. In contrast to the pronounced degree of apoptosis observed in NGP and SK-N-SH cells following Ad.CMV-*hPNPase*$^{old-35}$ and Ad.PEG-*hPNPase*$^{old-35}$ infection, transduction of SHEP cells with these viruses resulted in only a limited increase in the A_0 population, along with a slight G_1 arrest (Fig. 4C).

The induction of apoptosis by Ad.CMV-*hPNPase*$^{old-35}$ and Ad.PEG-*hPNPase*$^{old-35}$ infection of NGP and SK-N-SH cells was confirmed by analysis of caspase-3 and caspase-7 activity (Fig. 5). Adenovirus-mediated *hPNPase*$^{old-35}$ expression evoked a 2- to 3-fold and a 3- to 5-fold increase in caspase-3 and caspase-7 activity in NGP and SK-N-SH cells, respectively, measured 2-3 days after infection at 100 pfu/cell. No activation of these apoptotic effector enzymes was recorded in Ad.*vec*-infected NGP and SK-N-SH cells. Exposure of SHEP cells to Ad.CMV-*hPNPase*$^{old-35}$ and Ad.PEG-*hPNPase*$^{old-35}$ at 100 pfu/cell did not induce caspase-3 and caspase-7 activity, in keeping with the limited growth-suppressive effects that were observed using MTT assays.

Interestingly, microscopic evaluation of adenovirally infected NGP cells revealed striking morphological changes indicative of neuronal differentiation, such as the acquisition of a

bipolar or stellate appearance, and the formation of long neurites with varicosities and growth cone-like endings (Fig. 6A). These alterations were observed after infection of NGP cells with either of the evaluated adenoviruses (Ad.*vec*, Ad.CMV-*hPNPase*$^{old-35}$, and Ad.PEG-*hPNPase*$^{old-35}$), but not after transduction of any other cell type in this study. Confirmation of the neuronal differentiation process following adenoviral infection of NGP cells was obtained by expression analysis of neuronal differentiation markers using real-time quantitative RT-PCR (Fig. 6B). Adenoviral infection of NGP cells resulted in a marked increase in expression of the genes encoding the heavy, light, and medium neurofilament subunits (*NEFH*, *NEFL*, and *NEFM*, respectively) and of the rate-limiting enzyme in the biosynthesis of acetylcholine (*CHAT*), suggestive of differentiation along a cholinergic neuronal lineage.

Collectively, these data demonstrate that adenoviral infection of neuroblastoma cells results in a G_1 cell cycle arrest, which was accompanied by neuronal differentiation in NGP cells, that *hPNPase*$^{old-35}$ expression triggers a pronounced apoptotic response in NGP and SK-N-SH cells, and that the limited growth-inhibitory activity of *hPNPase*$^{old-35}$ gene delivery in SHEP cells correlates with a lack of apoptosis induction.

Discussion

The poor survival rates of high-risk neuroblastoma patients and the long-term severe side effects of current treatment regimens clearly warrant development of more effective and less toxic therapeutic modalities. Gene therapy holds great promise to improve the treatment of cancer, as gene transfer offers in principle the most direct and rational means to counteract the multiplicity of genetic events underlying the neoplastic process or to bring about destruction or incapacitation of tumor cells. Efforts to develop gene therapeutic approaches for treatment of neuroblastoma have been relatively limited to date. The present study was undertaken to evaluate a promising growth-inhibitory gene, *hPNPase*$^{old\text{-}35}$, operative through a mechanism completely different from those of conventional chemotherapeutic drugs, as a potential therapeutic agent for neuroblastoma, using adenovirus-mediated gene delivery with transgene expression driven by either the CMV promoter or by a cancer-selective promoter derived from the *PEG-3* gene. Our findings support the concept that *hPNPase*$^{old\text{-}35}$ is a negative regulator of growth and survival of neuroblastoma cells and that this gene may be exploited for an adenovirus-based gene therapy approach of neuroblastoma.

A prerequisite for a successful therapeutic modality is selective activity in tumor cells with minimal damage to normal cells. FM-516-SV immortalized normal melanocytes, which are, similarly to neuroblastoma cells, embryonically derived from the neural crest, were only to a limited extent suppressed in their growth after infection with Ad.CMV-*hPNPase*$^{old\text{-}35}$, despite a clear induction of *hPNPase*$^{old\text{-}35}$ expression. In contrast, most

neuroblastoma cell types showed pronounced growth inhibition after transduction with Ad.CMV-*hPNPase*$^{old-35}$. As selective delivery of genes to cancer cells remains one of the major hurdles to clinical implementation of gene therapy approaches, we decided to combine the growth-inhibitory effect of *hPNPase*$^{old-35}$ with the wide-ranging cancer-selective activity of the *PEG-3* promoter (Su et al., 2005). Use of the latter promoter induced a marked dose-dependent expression of *hPNPase*$^{old-35}$ and a profound growth suppression in IMR-32, NGP and SK-N-SH neuroblastoma cells, suggesting eligibility of a substantial fraction of neuroblastoma cases for treatment with *PEG-3* promoter-based gene therapy regimens.

The precise mechanism of the cancer selectivity and resulting favorable therapeutic index of the various antitumor ribonucleases described thus far remains to be elucidated (Benito et al., 2005; Arnold and Ulbrich-Hofmann, 2006). With regard to *hPNPase*$^{old-35}$, we previously documented its ability to selectively degrade c-*myc* mRNA as essential to the growth arrest induced by Ad.CMV-*hPNPase*$^{old-35}$ infection or IFN-β treatment of melanoma cells (Sarkar et al., 2003, 2006). We therefore investigated whether *hPNPase*$^{old-35}$ was also capable of specifically degrading N-*myc* mRNA in neuroblastoma cells, but this appears not to be the case (data not shown) and this would not have explained the excellent growth-inhibitory and proapoptotic activity of adenovirus-mediated *hPNPase*$^{old-35}$ gene transfer against the N-*myc* single-copy SK-N-SH cells. It is possible that a preferential degradation of other mRNA species encoding key proteins in neuroblastoma cell maintenance underlies the cytotoxic effect of *hPNPase*$^{old-35}$ on neuroblastoma cells. Additional research to unravel determinants of the substrate

specificity of *hPNPase*$^{old-35}$ activity will be needed to clarify this issue. Alternatively, it might be that malignant neuroblastoma cells are more dependent than normal cells on the overall integrity of their RNA due to their high proliferative and metabolic rate or due to collateral proapoptotic signals derived from the myriad of stresses to which tumor cells are subjected. Another explanation for the observed tumor selectivity of *hPNPase*$^{old-35}$ relates to the possibility of degradation of microRNAs (miRNAs), as has been postulated previously for other cytotoxic ribonucleases (Ardelt et al., 2003), since cumulating evidence indicates that miRNAs are deeply implicated in tumor biology but of considerably less importance in fully-developed normal cells.

A more thorough understanding of the molecular mode of action of *hPNPase*$^{old-35}$ might also shed light on the relatively resistant phenotype of SHEP cells. It is worth noting that these cells also have a poor response to irradiation (Jasty et al., 1998; Tweddle et al., 2001) and to various cytotoxic agents (unpublished observations), pointing at a more general insensitivity of SHEP cells to certain cell death-inducing triggers. This might for instance be related to a yet undefined block on apoptotic effector pathways in SHEP cells (Jasty et al., 1998), but an alternative hypothesis involves the poor tumorigenicity of these cells. SHEP cells, although widely used in neuroblastoma research, do neither form colonies in soft agar nor tumors when injected in nude mice (Ross and Spengler, 2007), and hence it can be questioned whether these tumor-derived cells still represent true malignant cells. In such a scenario, it is not surprising that the response of SHEP cells to adenovirus-mediated *hPNPase*$^{old-35}$ gene transfer resembles more closely the slight

growth suppression induced in FM-516-SV immortalized normal melanocytes than the strong apoptotic response of highly malignant neuroblastoma cells.

Interestingly, the process of adenoviral infection was sufficient to induce neuronal differentiation of NGP cells. Neuroblastoma is thought to arise from precursor cells of the sympathoadrenal system that are arrested at a developmental stage prior to completion of lineage maturation (McConville and Forsyth, 2003). As such, it is not unexpected that the induction of cell cycle arrest by adenoviral infection, which was observed in all cell lines evaluated, might be coupled with resumption of execution of the differentiation program. The observation of adenovirus-induced neuronal differentiation of NGP cells is however of interest from a clinical perspective, as it opens the possibility that some neuroblastoma tumors may mature after treatment with an adenovirus-based gene therapy approach.

In summary, our results indicate that *hPNPase*$^{old-35}$ may have utility for gene-based therapy of neuroblastoma and that the *PEG-3* promoter may provide a valuable tool for selective gene delivery to most neuroblastoma cells. Further studies in experimental animal models of neuroblastoma are essential to successfully translate this approach into a viable therapeutic strategy for neuroblastoma.

Acknowledgments

The present study was supported in part by National Institutes of Health grants P01 CA104177, R01 CA035675 and R01 CA102321, and the Samuel Waxman Cancer Research Foundation. T.V.M. is a research assistant from the Research Foundation – Flanders (FWO) and was supported by an FWO travel grant for this work. D.S. is the Harrison Endowed Scholar in Cancer Research. P.B.F. holds the Thelma Newmeyer Corman Chair in Cancer Research. W.A.W. and P.B.F. are Samuel Waxman Cancer Research Foundation Investigators. We thank Eun-Sook Park for adenovirus production and Justine Nuytens for assistance with real-time quantitative RT-PCR.

Literature Cited

Ardelt B, Ardelt W, Darzynkiewicz Z. 2003. Cytotoxic ribonucleases and RNA interference (RNAi). Cell Cycle 2(1):22-24.

Arnold U, Ulbrich-Hofmann R. 2006. Natural and engineered ribonucleases as potential cancer therapeutics. Biotechnol Lett 28(20):1615-1622.

Beck AK, Pass HI, Carbone M, Yang H. 2008. Ranpirnase as a potential antitumor ribonuclease treatment for mesothelioma and other malignancies. Future Oncol 4(3):341-349.

Benito A, Ribo M, Vilanova M. 2005. On the track of antitumour ribonucleases. Mol Biosyst 1(4):294-302.

Brodeur GM. 2003. Neuroblastoma: biological insights into a clinical enigma. Nat Rev Cancer 3(3):203-216.

Chan I, Lebedeva IV, Su ZZ, Sarkar D, Valerie K, Fisher PB. 2008. Progression elevated gene-3 promoter (PEG-Prom) confers cancer cell selectivity to human polynucleotide phosphorylase (*hPNPase*$^{old-35}$)-mediated growth suppression. J Cell Physiol 215(2):401-409.

Cinatl J, Jr., Cinatl J, Kotchetkov R, Matousek J, Woodcock BG, Koehl U, Vogel JU, Kornhuber B, Schwabe D. 2000. Bovine seminal ribonuclease exerts selective cytotoxicity toward neuroblastoma cells both sensitive and resistant to chemotherapeutic drugs. Anticancer Res 20(2A):853-859.

Cinatl J, Jr., Cinatl J, Kotchetkov R, Vogel JU, Woodcock BG, Matousek J, Pouckova P, Kornhuber B. 1999. Bovine seminal ribonuclease selectively kills human

multidrug-resistant neuroblastoma cells via induction of apoptosis. Int J Oncol 15(5):1001-1009.

D'Alessio G. 1993. New and cryptic biological messages from RNases. Trends Cell Biol 3(4):106-109.

Hellemans J, Mortier G, De Paepe A, Speleman F, Vandesompele J. 2007. qBase relative quantification framework and software for management and automated analysis of real-time quantitative PCR data. Genome Biol 8(2):R19.

Holmes M, Rosenberg E, Valerie K. 2003. Adenovirus expressing p53. Methods Mol Biol 234:1-16.

Jasty R, Lu J, Irwin T, Suchard S, Clarke MF, Castle VP. 1998. Role of p53 in the regulation of irradiation-induced apoptosis in neuroblastoma cells. Mol Genet Metab 65(2):155-164.

Kotchetkov R, Cinatl J, Matousek J, Vogel J, Pouckova P, Wagner M, Kornhuber B, Schwabe D, Cinatl J, Jr. 2000. Bovine seminal ribonuclease inhibits in vivo growth of human neuroblastoma cells. Oncol Rep 7(2):363-367.

Lebedeva IV, Sarkar D, Su ZZ, Kitada S, Dent P, Stein CA, Reed JC, Fisher PB. 2003. Bcl-2 and Bcl-x_L differentially protect human prostate cancer cells from induction of apoptosis by melanoma differentiation associated gene-7, *mda*-7/IL-24. Oncogene 22(54):8758-8773.

Lebedeva IV, Su ZZ, Chang Y, Kitada S, Reed JC, Fisher PB. 2002. The cancer growth suppressing gene *mda*-7 induces apoptosis selectively in human melanoma cells. Oncogene 21(5):708-718.

Leszczyniecka M, Kang DC, Sarkar D, Su ZZ, Holmes M, Valerie K, Fisher PB. 2002. Identification and cloning of human polynucleotide phosphorylase, *hPNPase*$^{old-35}$, in the context of terminal differentiation and cellular senescence. Proc Natl Acad Sci U S A 99(26):16636-16641.

Leszczyniecka M, Su ZZ, Kang DC, Sarkar D, Fisher PB. 2003. Expression regulation and genomic organization of human polynucleotide phosphorylase, *hPNPase*$^{old-35}$, a Type I interferon inducible early response gene. Gene 316:143-156.

Maris JM, Hogarty MD, Bagatell R, Cohn SL. 2007. Neuroblastoma. Lancet 369(9579):2106-2120.

McConville CM, Forsyth J. 2003. Neuroblastoma – a developmental perspective. Cancer Lett 197(1-2):3-9.

Michaelis M, Cinatl J, Anand P, Rothweiler F, Kotchetkov R, Deimling A, Doerr HW, Shogen K, Cinatl J, Jr. 2007. Onconase induces caspase-independent cell death in chemoresistant neuroblastoma cells. Cancer Lett 250(1):107-116.

Pattyn F, Robbrecht P, De Paepe A, Speleman F, Vandesompele J. 2006. RTPrimerDB: the real-time PCR primer and probe database, major update 2006. Nucleic Acids Res 34(Database issue):D684-688.

Pattyn F, Speleman F, De Paepe A, Vandesompele J. 2003. RTPrimerDB: the real-time PCR primer and probe database. Nucleic Acids Res 31(1):122-123.

Ross RA, Spengler BA. 2007. Human neuroblastoma stem cells. Semin Cancer Biol 17(3):241-247.

Sarkar D, Fisher PB. 2006. Polynucleotide phosphorylase: an evolutionary conserved gene with an expanding repertoire of functions. Pharmacol Ther 112(1):243-263.

Sarkar D, Lebedeva IV, Emdad L, Kang DC, Baldwin AS, Jr., Fisher PB. 2004. Human polynucleotide phosphorylase (*hPNPase*$^{old-35}$): a potential link between aging and inflammation. Cancer Res 64(20):7473-7478.

Sarkar D, Leszczyniecka M, Kang DC, Lebedeva IV, Valerie K, Dhar S, Pandita TK, Fisher PB. 2003. Down-regulation of Myc as a potential target for growth arrest induced by human polynucleotide phosphorylase (*hPNPase*$^{old-35}$) in human melanoma cells. J Biol Chem 278(27):24542-24551.

Sarkar D, Park ES, Barber GN, Fisher PB. 2007. Activation of double-stranded RNA–dependent protein kinase, a new pathway by which human polynucleotide phosphorylase (*hPNPase*$^{old-35}$) induces apoptosis. Cancer Res 67(17):7948-7953.

Sarkar D, Park ES, Emdad L, Randolph A, Valerie K, Fisher PB. 2005. Defining the domains of human polynucleotide phosphorylase (hPNPase^{OLD-35}) mediating cellular senescence. Mol Cell Biol 25(16):7333-7343.

Sarkar D, Park ES, Fisher PB. 2006. Defining the mechanism by which IFN-β dowregulates c-*myc* expression in human melanoma cells: pivotal role for human polynucleotide phosphorylase (*hPNPase*$^{old-35}$). Cell Death Differ 13(9):1541-1553.

Su ZZ, Sarkar D, Emdad L, Duigou GJ, Young CS, Ware J, Randolph A, Valerie K, Fisher PB. 2005. Targeting gene expression selectively in cancer cells by using the progression-elevated gene-3 promoter. Proc Natl Acad Sci U S A 102(4):1059-1064.

Tweddle DA, Malcolm AJ, Cole M, Pearson AD, Lunec J. 2001. p53 cellular localization and function in neuroblastoma: evidence for defective G_1 arrest despite WAF1 induction in MYCN-amplified cells. Am J Pathol 158(6):2067-2077.

Van Maerken T, Speleman F, Vermeulen J, Lambertz I, De Clercq S, De Smet E, Yigit N, Coppens V, Philippe J, De Paepe A, Marine JC, Vandesompele J. 2006. Small-molecule MDM2 antagonists as a new therapy concept for neuroblastoma. Cancer Res 66(19):9646-9655.

Vandesompele J, De Paepe A, Speleman F. 2002a. Elimination of primer-dimer artifacts and genomic coamplification using a two-step SYBR green I real-time RT-PCR. Anal Biochem 303(1):95-98.

Vandesompele J, De Preter K, Pattyn F, Poppe B, Van Roy N, De Paepe A, Speleman F. 2002b. Accurate normalization of real-time quantitative RT-PCR data by geometric averaging of multiple internal control genes. Genome Biol 3(7):RESEARCH0034.

Vasandani VM, Burris JA, Sung C. 1999. Reversible nephrotoxicity of onconase and effect of lysine pH on renal onconase uptake. Cancer Chemother Pharmacol 44(2):164-169.

Vasandani VM, Wu YN, Mikulski SM, Youle RJ, Sung C. 1996. Molecular determinants in the plasma clearance and tissue distribution of ribonucleases of the ribonuclease A superfamily. Cancer Res 56(18):4180-4186.

Youle RJ, Newton D, Wu YN, Gadina M, Rybak SM. 1993. Cytotoxic ribonucleases and chimeras in cancer therapy. Crit Rev Ther Drug Carrier Syst 10(1):1-28.

Young IT. 1977. Proof without prejudice: use of the Kolmogorov-Smirnov test for the analysis of histograms from flow systems and other sources. J Histochem Cytochem 25(7):935-941.

Figure legends

Figure 1. Infection with Ad.CMV-*GFP* induces GFP expression in neuroblastoma cells. A panel of five human neuroblastoma cell lines [IMR-32, NGP, SHEP, SK-N-BE(2c), and SK-N-SH], DU-145 human prostate carcinoma cells, and FM-516-SV immortalized human melanocytes were infected with Ad.CMV-*GFP* at the indicated MOIs, and analyzed for the expression of GFP 24 h postinfection using flow cytometry. Columns represent the mean percentages of GFP-positive cells of three different experiments, and error bars indicate standard errors of the mean. Asterisk, percentage of GFP-positive cells 24 h after mock infection ranged from 0.19% to 0.22% for all cell lines.

Figure 2. Expression of *hPNPase*$^{old-35}$ in FM-516-SV human melanocytes and neuroblastoma cells following adenoviral gene transfer. FM-516-SV immortalized melanocytes and a panel of five neuroblastoma cell lines were infected with Ad.*vec*, Ad.CMV-*hPNPase* (Ad.CMV-*hPNPase*$^{old-35}$; hemagglutinin [HA]-tagged *hPNPase*$^{old-35}$ expression driven by the CMV promoter), or Ad.PEG-*hPNPase* (Ad.PEG-*hPNPase*$^{old-35}$; HA-tagged *hPNPase*$^{old-35}$ expression driven by the *PEG-3* promoter) at the indicated MOIs, and probed 48 h postinfection for *hPNPase*$^{old-35}$ expression by Western blot analysis using an anti-HA antibody. Expression of EF1α is shown as loading control.

Figure 3. Effect of Ad.*vec*, Ad.CMV-*hPNPase*$^{old-35}$, and Ad.PEG-*hPNPase*$^{old-35}$ on growth and viability of FM-516-SV human melanocytes and neuroblastoma cells. Exponentially growing cells were untreated or infected with Ad.*vec*, Ad.CMV-*hPNPase*

(Ad.CMV-*hPNPase*$^{old-35}$), or Ad.PEG-*hPNPase* (Ad.PEG-*hPNPase*$^{old-35}$) at 100 pfu/cell, and the number of viable cells was determined at 1, 3 and 5 days postinfection using MTT assay. Points represent the mean relative numbers of viable cells of three independent experiments, and error bars indicate standard errors of the mean.

Figure 4. Effect of Ad.*vec*, Ad.CMV-*hPNPase*$^{old-35}$, and Ad.PEG-*hPNPase*$^{old-35}$ on cell cycle distribution and hypodiploid DNA content of human neuroblastoma cells. NGP (A), SK-N-SH (B), and SHEP (C) cells were untreated or infected with Ad.*vec*, Ad.CMV-*hPNPase* (Ad.CMV-*hPNPase*$^{old-35}$), or Ad.PEG-*hPNPase* (Ad.PEG-*hPNPase*$^{old-35}$) at 100 pfu/cell, harvested at 2, 3, 4 and 5 days postinfection, and monitored for DNA content by propidium iodide staining and flow cytometric analysis. Columns represent the mean cell cycle and apoptotic fractions of three different experiments, and error bars correspond to standard errors of the mean.

Figure 5. Effect of Ad.*vec*, Ad.CMV-*hPNPase*$^{old-35}$, and Ad.PEG-*hPNPase*$^{old-35}$ on caspase-3 and caspase-7 activity in human neuroblastoma cells. NGP, SK-N-SH, and SHEP cells were untreated or infected with Ad.*vec*, Ad.CMV-*hPNPase* (Ad.CMV-*hPNPase*$^{old-35}$), or Ad.PEG-*hPNPase* (Ad.PEG-*hPNPase*$^{old-35}$) at 100 pfu/cell, and the combined activity of caspase-3 and caspase-7, relative to uninfected cells, was determined at 2 and 3 days postinfection. Columns represent the mean caspase-3 and caspase-7 activity values of triplicate wells, and error bars correspond to standard deviations.

Figure 6. Adenoviral infection induces neuronal differentiation of NGP human neuroblastoma cells. A: Phase-contrast images of NGP cells left untreated for five days (*left*) and five days after infection with Ad.*vec* (*right*). Adenoviral infection induced clear morphogical signs of neuronal differentiation, including a polar morphology and extensive outgrowth of neuritic processes, which formed a netlike arrangement. Similar morphological changes were observed after infection of NGP cells with Ad.CMV-*hPNPase*$^{old\text{-}35}$ or Ad.PEG-*hPNPase*$^{old\text{-}35}$ (not shown). B: Real-time quantitative RT-PCR analysis of expression of neuronal differentiation markers (*NEFH*, *NEFL*, *NEFM*, and *CHAT*) in NGP cells harvested five days after exposure to control conditions or to infection with Ad.*vec*, Ad.CMV-*hPNPase* (Ad.CMV-*hPNPase*$^{old\text{-}35}$), or Ad.PEG-*hPNPase* (Ad.PEG-*hPNPase*$^{old\text{-}35}$) at 100 pfu/cell. Columns represent the mean mRNA expression levels derived from two RT-PCR measurements, and error bars indicate standard deviations.

Table 1. Expression of coxsackie-adenovirus receptors (CAR) on the surface of DU-145 prostate carcinoma cells, FM-516-SV immortalized melanocytes, and neuroblastoma cells

	DU-145	FM-516-SV	IMR-32	NGP	SHEP	SK-N-BE(2c)	SK-N-SH
D value	0.88	0.42	0.68	0.79	0.53	0.33	0.54
Peak shift	4.66	0.61	1.72	1.34	1.30	0.74	1.23

Cells were incubated with mouse monoclonal anti-CAR antibody, washed, stained with FITC-labeled anti-mouse immunoglobulins, washed, analyzed by flow cytometry, and compared with a number of appropriate controls, as described in Material and Methods. The *D* value, calculated by the Kolmogorov-Smirnov two-sample test for analysis of flow cytometric histograms and reflecting the greatest difference between the cumulative distribution functions derived from the histograms (Young, 1977), indicated for all cell types in this study the presence of CAR surface expression at the 99.9% confidence level. The peak shift, computed as a ratio $(P_{CAR} - P_{ctrl})/P_{ctrl}$ with P_{CAR} and P_{ctrl} being the median of the fluorescent peak of the flow cytometric histogram of the CAR-stained cells and of the control cells with the highest FITC signal intensity, respectively, allows for comparison of surface CAR number and availability between different cell types.

Figure 1 - Van Maerken *et al.*

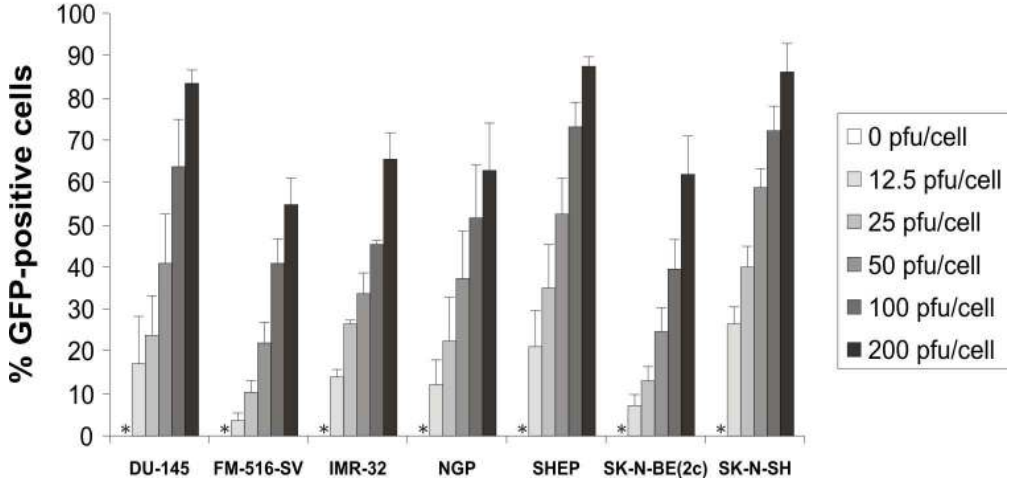

128x78mm (300 x 300 DPI)

Figure 2 - Van Maerken *et al.*

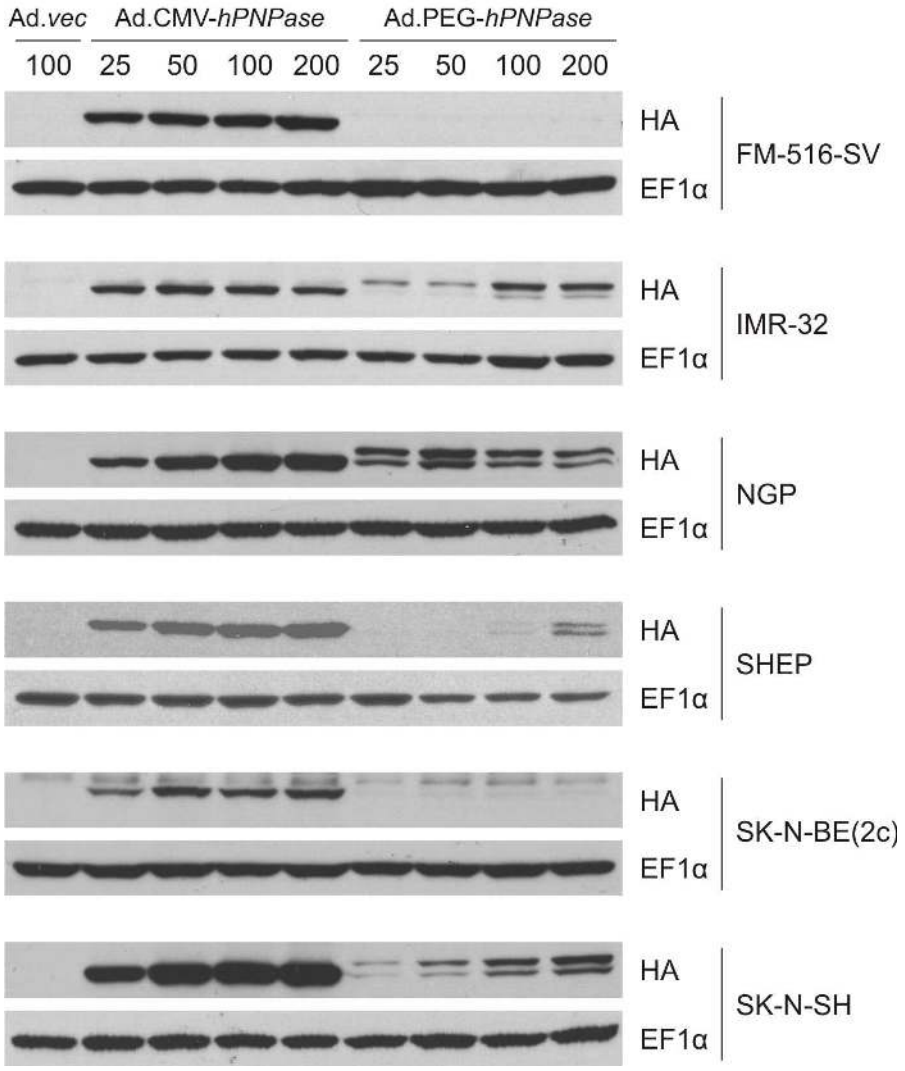

111x149mm (300 x 300 DPI)

Figure 3 - Van Maerken *et al.*

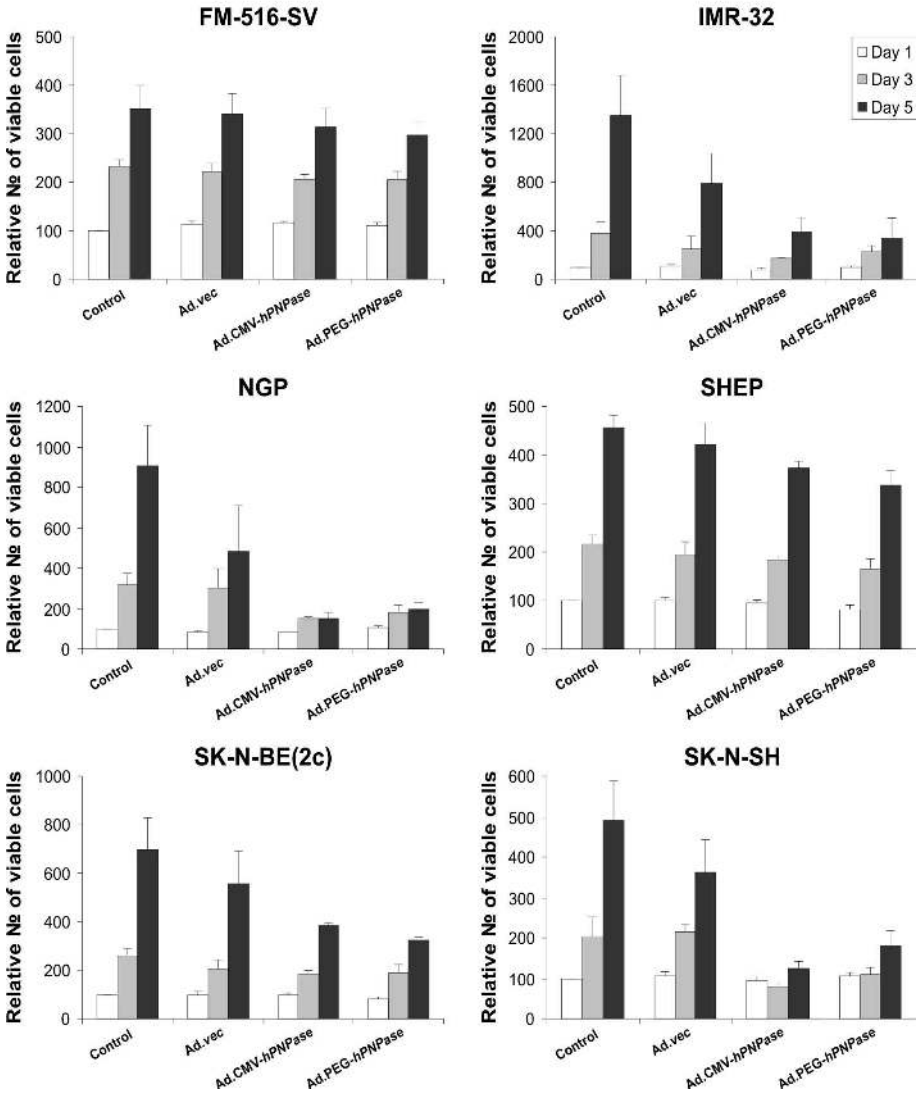

135x178mm (300 x 300 DPI)

Figure 4 - Van Maerken *et al.*

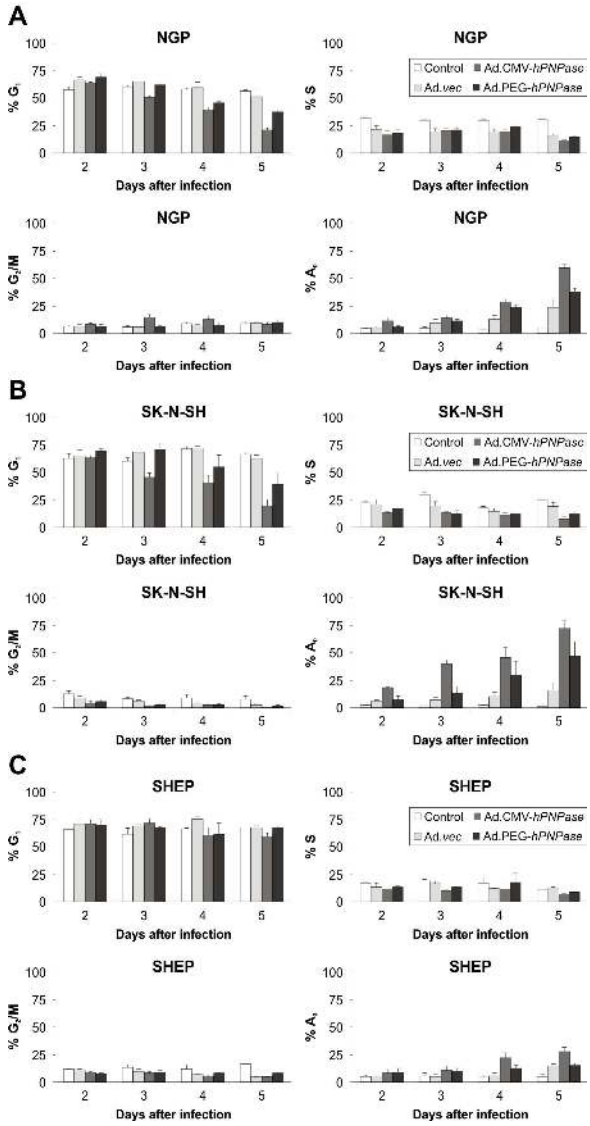

120x249mm (300 x 300 DPI)

Figure 5 - Van Maerken *et al.*

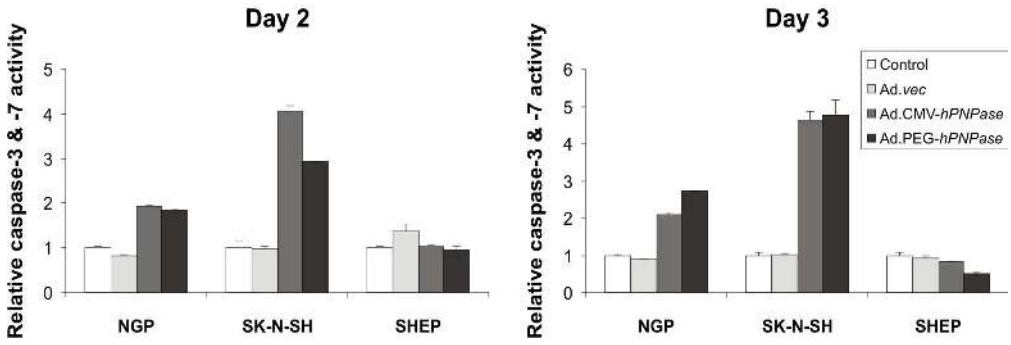

138x63mm (300 x 300 DPI)

Figure 6 - Van Maerken *et al.*

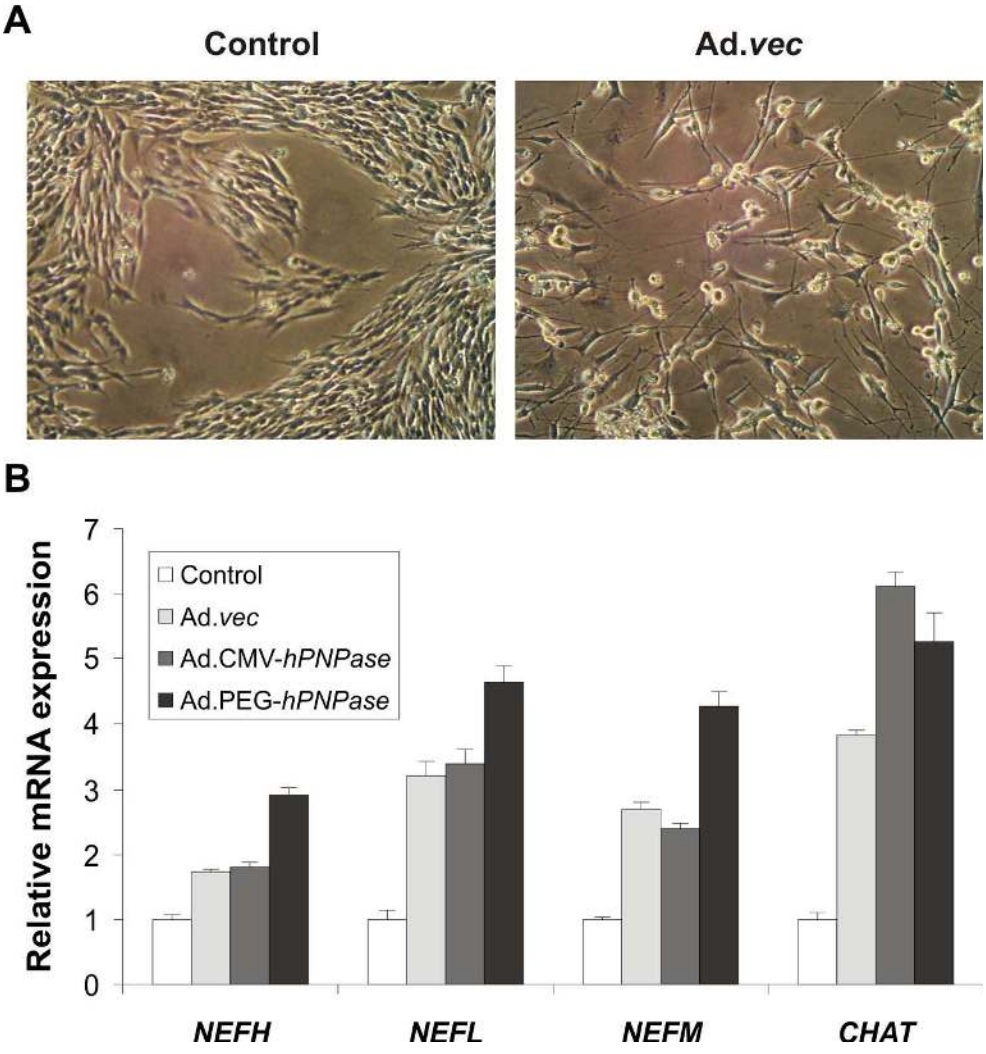

106x130mm (300 x 300 DPI)